

On the feasibility of friction spot joining in magnesium/fiber-reinforced polymer composite hybrid structures

S.T. Amancio-Filho^{a,*}, C. Bueno^{a,b}, J.F. dos Santos^a, N. Huber^a, E. Hage Jr.^b

^a Helmholtz-Zentrum Geesthacht, Institute of Materials Research, Materials Mechanics, Max-Planck-Str. 1, D-21502 Geesthacht, Germany

^b Federal University of Sao Carlos (UFSCar), Department of Materials Engineering (DEMa), Rodovia Washington Luiz km 235, 13565-905 Sao Carlos, SP, Brazil

ARTICLE INFO

Article history:

Received 29 October 2010

Received in revised form 20 January 2011

Accepted 21 January 2011

Available online 28 January 2011

Keywords:

Magnesium alloys

Polymers

Composites

Welding

Bonding

Interfaces

ABSTRACT

In the present study, the feasibility of the friction spot joining technique on magnesium AZ31–O/glass fiber and carbon fiber reinforced poly(phenylene sulfide) joints is addressed. The thermo-mechanical phenomena associated with the friction spot joining process promoted metallurgical and polymer physical-chemical transformations. These effects resulted in grain refinement by dynamic recrystallization and changes in local (microhardness) and global strength (lap shear). Friction spot lap joints with elevated mechanical performance (20–28 MPa) were produced without surface pre-treatment. This preliminary investigation has successfully shown that friction spot joining is an alternative technology for producing hybrid polymer-metal structures.

© 2011 Elsevier B.V. All rights reserved.

1. Introduction

The increasing levels of CO₂ emissions from transportation have become an urgent societal matter. This is mainly related to the growth of overall vehicle weight because of increased safety and passenger comfort requirements [1]. The selection and development of lightweight materials, such as magnesium [2] and advanced polymer-based materials, such as carbon fiber-reinforced thermoplastics (CFRT) [4], can result in reductions in vehicle weight. These materials are combined with the aim of increasing the weight-to-strength structural performance of transportation components and reducing both fuel consumption and gas emissions [3–6]. Joining technology is a key technique for fabricating polymer-metal hybrid components because of the many technical and manufacturing problems associated with making large structures (e.g., high levels of physical-chemical dissimilarity [7]). Messler [8,9] has recently reported that the joining methods used for polymer-metal hybrid structures are mechanical fastening, adhesive bonding, welding (e.g., resistance and induction welding), and riveting processes. However, these current joining techniques have been identified as either application-specific or limited in performance, or they are not environmental friendly [10]. Therefore, there is a niche for innovative joining technologies designed for this

purpose. Friction spot welding, FSpW—also known as refill-spot welding, is a solid-state welding technique for lightweight metals developed at GKSS Research Centre, Geesthacht [11]. The latest investigations by Oliveira et al. [12] have demonstrated the feasibility of FSpW on thermoplastics. Amancio-Filho et al. [13] have recently shown that thermoplastics can be joined to metals by a new joining method based on FSpW called friction spot joining, FSpJ [14].

In the current work, the feasibility of FSpJ on short-fiber and woven-reinforced thermoplastic composites connected to lightweight metals is presented through a case study on two different commercially available materials, a magnesium alloy (AZ31B) and two thermoplastic composites (glass fiber- and carbon fiber-reinforced poly(phenylenesulfide), PPS). These materials are increasingly chosen for structural applications in transportation. The AZ31 alloy is a ternary (MgAl₃Zn₁), wrought magnesium alloy used mainly as hot-rolled sheets in automotive applications [15]. It presents low density, high specific strength, and fairly good welding ability by traditional [16] and solid-state joining methods [17–19]. PPS is a semi-crystalline engineering thermoplastic displaying high thermal stability (maximum service temperature in air of 170–260 °C) and resistance (deflection temperature at 8 MPa of 95 °C), chemical resistance, high dimensional stability, and low moisture absorption [20]. Due to its high processing temperatures (decomposition starting at 500 °C [21]), this plastic is a good candidate for welding applications [21]. Glass fiber-reinforced PPS (PPS-GF) is usually applied in the fabrication of electrical

* Corresponding author. Tel.: +49 4152 87 2066; fax: +49 4152 87 2033.

E-mail address: sergio.amancio@hzg.de (S.T. Amancio-Filho).

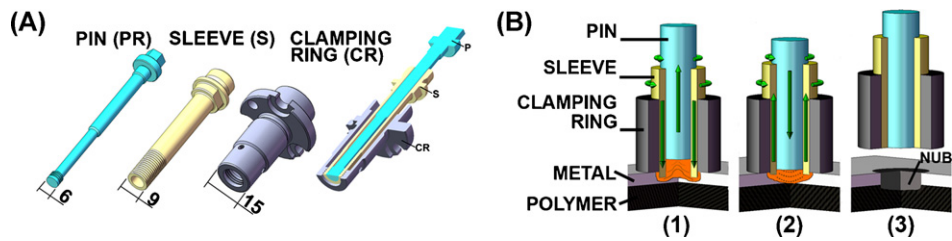


Fig. 1. (A) Illustration of the FSpW tools used in this work (dimensions in mm). (B) Schematic description of the “Sleeve Plunge” FSpJ-variant: (1) sleeve plunging and plasticizing of the metallic material; (2) spot refilling; (3) joint consolidation.

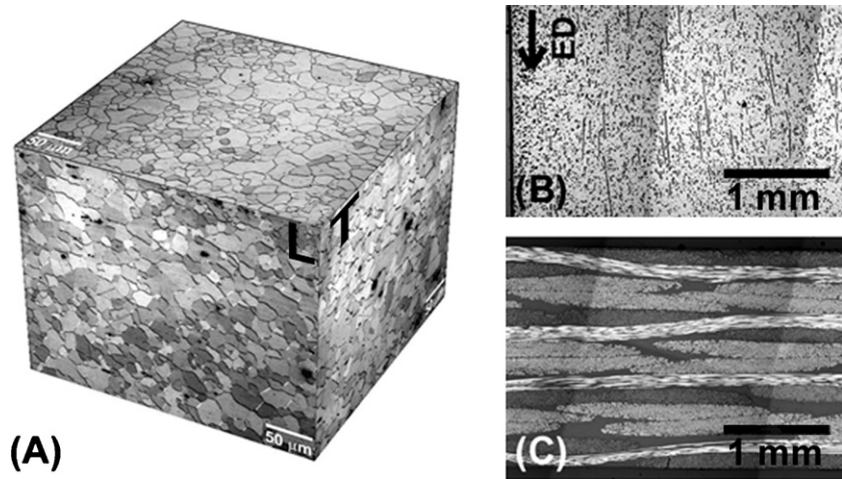


Fig. 2. (A) 3D schematic representation of the microstructure of the AZ31–O base material (L: longitudinal, T: transversal), (B) microstructure of PPS–GF (40% short fibers) in the extrusion direction (ED) and (C) PPS–CF (5H satin, carbon-fiber woven reinforced) composites used in this work.

components in automotive parts [22]. Carbon fiber-reinforced PPS (PPS–CF) is mainly utilized in aircraft structural applications, such as in J-Nose wing substructures [23].

This work describes the main features of the FSpJ technique. Selected results on temperature history, microstructure, local (microhardness) and global (lap shear strength) performance are discussed to demonstrate the process feasibility and to illustrate the main characteristics of AZ31/PPS–GF and PPS–CF spot joints.

2. Principles of joining polymer–metal hybrid structures by friction spot joining (FSpJ)

FSpJ uses a three-piece, non-consumable tool system comprising a clamping ring, a shoulder, and a pin (Fig. 1A). The tool components are mounted coaxially and can be rotated and moved in and out independently of each another. Analogous to friction spot welding of metals, FSpJ of polymer–metal structures has two variants: the “Sleeve Plunge” (Fig. 1B) and “Pin Plunge” (not depicted). In the “Sleeve Plunge” variant, the joining pieces are initially overlapped and clamped between a backing plate and the clamping ring with the metal piece on top of the polymeric partner. Sleeve and

pin begin to rotate in the same direction. Then the sleeve touches down on the upper surface of the metal piece producing frictional heat. Concomitantly, the sleeve is inserted into the metal piece and the pin retracted, forming an annular space or reservoir (Fig. 1B-1). During the sleeve plunging step, thermally plasticized metal is squeezed into the created reservoir.

At the end of the joining time, the sleeve is retracted from the surface of the metallic piece while the pin pushes the entrapped plasticized metallic material (Fig. 1B-2) back, refilling the key hole. The tool plunging depth is set to prevent damage to the polymeric piece. Plunging takes place only in the metallic partner. This is intended to avoid or reduce damage to the fiber reinforcement, which can decrease the joint performance. Moreover, the plasticized metallic partner is deformed by the tool plunging movement. This creates a metallic “nub” on the surface the polymeric piece (Fig. 1B-3). Frictional heat flows from the metallic to the polymeric partner by conduction, and a thin layer of molten/softened polymer is created underneath the spot surface. In the case of reinforced plastics and polymer composites, the fiber network is slightly displaced to the edges of the spot. Finally, the joining head is retracted, and the spot weld consolidates under pressure (Fig. 1B-3). In the

Table 1
Nominal chemical composition of AZ31B–O alloy used in this work.

wt%	Al	Zn	Mn	Cu	Si	Cr	Fe	Ti	Mg
Avg.	2.9	1.1	0.27	0.002	<0.01	<0.001	0.006	<0.0002	bal.

Table 2
Mechanical properties of AZ31B–O alloy used in this work.

Mechanical properties	Rp0.2 [MPa]	Rm [MPa]	A [%]	Microhardness [HV]
LT-direction (tensile)	170.6 ± 8.7	255.4 ± 1.5	19.8 ± 1.1	58,1 ± 0,4
TL-direction (tensile)	186.1 ± 1.2	256.4 ± 0.9	16.0 ± 1.1	

Table 3

Physical properties of AZ31B–O alloy used in this work [24].

Liquidus temperature [°C]	Solidus temperature [°C]	Insipient melting temperature [°C]	Thermal conductivity at 20 °C [W m ⁻¹ K ⁻¹]	Coefficient of thermal expansion within 20–200 °C [mm ⁻¹ K ⁻¹]
632	566	532	76,9	26,8

“Pin Plunge” variant (not depicted), the pin penetrates the metal piece while the sleeve is retracted. The other process steps are equivalent to the “Sleeve Plunge” variant.

3. Materials and methods

3.1. Base materials

3.1.1. Magnesium AZ31

Two-millimeter rolled magnesium AZ31B sheets in the temper condition “O” (annealed and recrystallized in accordance to [24]) were used in this work. The nominal chemical composition of this Mg–Al–Zn alloy was determined by chemical analysis and is presented in Table 1. The average experimental yield, ultimate tensile strength, elongation at fracture, and the average microhardness of this magnesium alloy at room temperature are presented in Table 2. The similarity of the tensile properties in the longitudinal (LT) and transverse (TL) orientations with respect to the rolling direction, and the low standard deviation of the average microhardness suggest a reduced anisotropy in mechanical properties.

The microstructure of the alloy AZ31 is shown in Fig. 2A for the longitudinal (L), transverse (T), and surface planes in relation to the rolling direction. The microstructure exhibits fine dynamically recrystallized grains as a result of hot rolling fabrication. Some darker spots at the grain boundaries are found randomly displaced throughout the sheet thickness. These features are most likely Mg₁₇Al₁₂ [24] or Al₃Mg₂ [25] intermetallic particles that commonly form in Mg–Al–Zn alloys during thermo-mechanical processing. These brittle particles contribute to the alloy strength by dictating the amount and size of dynamic recrystallized grains (i.e., retardation of grain growth by a pinning effect) [26], and they can also act as crack initiation sites [25]. The main physical properties of AZ31–O alloy relevant to the understanding of the joint microstructural changes associated with processing are given in Table 3.

3.1.2. PPS-GF and PPS-CF reinforced composites

Eight-millimeter extruded plates of PPS reinforced with 40 vol% short glass fibers (Techtron HPV, Quadrant Engineering Plastic Products, Germany) and 2.1-mm PPS-CF woven-reinforced laminates (5H Satin, [(0.90)/(±45)]₃/(0.90) and 43% fiber reinforcement in weight; Tencate, Netherlands) were selected for the hybrid joints. Table 4 presents the main mechanical and physical properties of the composites studied. The thermal conductivity of the PPS composites is 0.25–0.4% that of the AZ31–O magnesium alloy, whereas their coefficients of linear thermal expansion are about twice the value observed for the AZ31–O alloy. The large difference in thermal conductivity results in very complex heat flow and temperature distribution during joining, whereas the different

coefficients of linear thermal expansion can be detrimental to the joint mechanical strength. During cooling, the composite tends to separate from the metal because of thermal shrinkage. To avoid or reduce this effect, mechanical clamping is applied during the joint consolidation.

Although the ultimate tensile strength of the PPS-CF laminate is much higher than that of the PPS-GF composite (see Table 4), the in-plane shear strength is only 119 MPa [28], which is about half the tensile strength of AZ31. The decreased in-plane shear strength of the laminate limits the joint lap shear performance, which is normally lower than the tensile strength of the laminate composite. The general aspects of the microstructure of the PPS composites are presented in cross-sectional macrographs in Fig. 2B and C.

3.2. Experimental procedure

3.2.1. Microscopic analysis

Optical microscopy (OM) specimens were prepared from the base materials, and cross-sections were cut axially to the rivet length in the middle of joint with a low-speed saw (Buehler, Germany). Materialographic specimens were embedded in low cure-temperature epoxy resin (Epoxicure, Buehler, Germany) to avoid any thermal changes in the polymeric partner, and the specimens were grinded and polished according to standard procedures. Chemical etching of the AZ31 alloy was performed with an ethanol solution of picric and acetic acids in water (8 g picric acid, 5 mL acetic acid, 100 mL ethanol and 10 mL distilled water). OM was carried out under reflective non-polarized (DM IR microscope, Leica, Germany) and polarized light (PMG 3 microscope, Olympus, Germany). Polymer–metal interfaces were also investigated by laser microscopy (VK-9700 microscope, Keyence, Japan).

3.2.2. Mechanical testing

Vickers microhardness testing was performed in an automatic indenter (ZHV Zwick Roel, Germany) on embedded materialographic specimens under different conditions for the polymeric and metallic partners. For the AZ31 specimens, an indentation load of 200 gf (1.96 N) for 5 s and an indentation spacing of 0.5 mm [29] were utilized. A load of 50 gf (0.49 N) with 15 s of holding time (compensating for the visco-elastic behavior of this thermoplastic [30]) and 0.3 mm of indentation spacing were selected to test the PPS composites.

Base material and joint global mechanical strength were analyzed through lap shear testing according to DIN EN 10002 [31] (AZ31), DIN 53455 [32] (PPS-GF) and ASTM D 1002-05 [33] (overlap joints). Tensile and lap shear testing were performed in a universal testing machine with a traverse speed of 2 mm/min at room temperature.

Table 4

Room temperature mechanical and physical properties of PPS-GF and PPS-CF composites used in this work.

	Rm [MPa]	A [%]	Glass transition temperature [°C]	Melting temperature [°C]	Thermal conductivity at 23 °C [W m ⁻¹ K ⁻¹]	Coefficient of thermal expansion within 23–150 °C [mm ⁻¹ K ⁻¹]
PPS-GF	61.0 ± 1.0758 (warp)	4.9 ± 0.6	90 Ref. [27]	280 Ref. [27]	0.30 Ref. [27]	60 Ref. [27]
PPS-CF	755 (weft) Ref. [28]	3 Ref. [28]	120 Ref. [28]	280 Ref. [28]	0.19 Ref. [28]	52.2 Ref. [28]

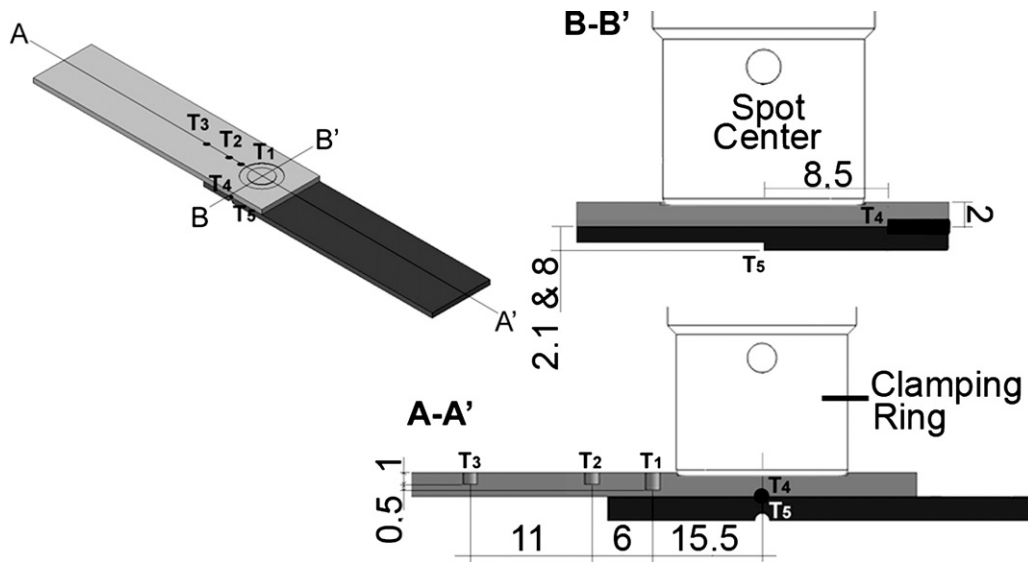


Fig. 3. Diagram of positioning of the thermocouples selected for thermometric measurements: A–A' is the longitudinal section, parallel to the specimen length, and B–B' is the transversal view.

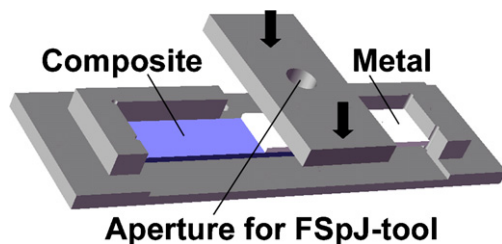


Fig. 4. Schematic representation of the sample holder and clamping system for overlap joints.

3.2.3. Thermal measurements

The process temperature was determined with an infrared camera (VarioTHERM camera, Jenoptik, Germany) set in the range of 200–500 °C, with a resolution of 256 × 256 pixels at 50 Hz. Thermocouples (type K Cr–Ni, 0.5 mm diameter) were embedded into the joining partners at five different positions, as illustrated in Fig. 3.

3.2.4. Joining procedure

Joints were produced in a friction spot welding instrument (Harms&Wende, Germany) equipped with a specimen clamping system (Fig. 4) designed for the production of single lap joints. Threaded tools (Fig. 1A) were fabricated from electroslag-remelted, maraging, warm-work tool steel 1.6358 (X2NiCoMo18-9-5). Prior to joining, AZ31 specimens were ground with P1200 SiC paper to remove the intrinsic Mg(OH)₂ layer. Both joint partners were cleaned with acetone. The optimal range of parameters for joining AZ31 to PPS-GF and to PPS-CF is summarized in Table 5. No additional treatment was applied to the surfaces prior to joining.

Table 5
Range of joining parameters for each combination of materials.

Parameter (unit)	AZ31/PPS-CF	AZ31/PPS-GF
Rotational speed (rpm)	900–3000	900–3000
Tool plunge depth (mm)	0.25–0.35	0.25–1.75
Joining time (s)	4–8	3–8
Joining pressure (bar)	2.4–3.0	2–3

4. Results and discussion

4.1. Temperature field formation

Fig. 5A presents selected results showing a typical temperature distribution in the clamping ring of a friction-spot joined PPS-CF/AZ31 single-lap connection (1500 rpm, 0.25 mm, 8 s and 3 bar). Temperatures within the regions closer to the magnesium plate exhibited the highest values varying between approximately 400 °C and 440 °C.

Fig. 5B shows thermometric results for the same joint. Thermocouple T1, which is the nearest measurement point to the metal plasticizing volume (8.25 mm from the spot center and 1.5 mm deep in the metal partner), gives the highest temperature values, of about 275 °C, followed by thermocouples T2 and T4 (13.25 mm from the spot center and 1 mm into the metal partner and 8.25 mm from the spot center and between partners, respectively), which registered temperatures around 170 °C and 225 °C, respectively. Thermocouples T3 and T5 presented the lowest maximum temperatures (120 °C and 90 °C, respectively). This is probably due to their distance from the heat source (23.25 mm from the spot center and 1 mm deep in the metal partner in the case of T3, whereas T5 was placed at the bottom of the PPS-CF plaque, in the middle of the spot center).

The peak temperatures measured represent 50–80% of the melting point of AZ31B, which is in accordance with temperatures measured during friction stir welding with similar process conditions [18,34]. This is within the range of dynamic metallurgical transformations for AZ31B [35]. In this way, microstructural changes are expected to occur during joining. The results of the temperature development for the PPS-CF composite–AZ31 joints indicated that the process temperature is directly proportional to the energy input. Comparable to friction spot welding of metals, energy input is dictated by the welding parameters, such as rotational speed, joining time and tool plunge rate. A parametric study of the relationship between energy input, temperature and process by statistical analysis is forthcoming.

4.2. Microstructure and local joint strength

Fig. 6 illustrates the surface view (Fig. 6A and C) and cross-sectional macrographs (Fig. 6B and D) of two sound

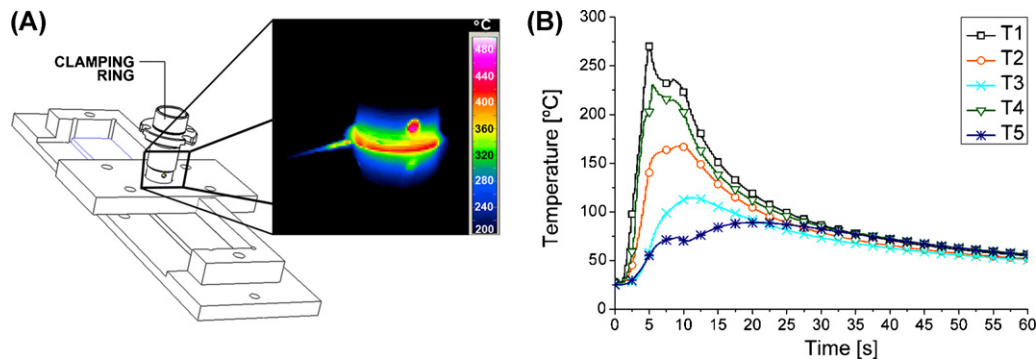


Fig. 5. Temperature history measured by (A) infrared thermography and (B) thermometry for a AZ31/PPS-CF joint (1500 rpm, 0.25 mm, 8 s and 3 bar).

FSpJ joints on PPS-CF, PPS-GF/Mg AZ31 base materials (PPS-CF joint: 1500 rpm/0.25 mm/8 s/3 bar and PPS-GF joint 3000 rpm/0.25 mm/8 s/2 bar).

From the surface overview (Fig. 6A and C), it is possible to identify the typical pattern of two concentric rings left by the tool in the spot area. The internal ring consists of the stirred material, whereas the external ring is the impression left by the clamping ring. From the cross-sectional view in Fig. 6B, one observes a deformed metallic volume forming a “nub” inserted into the polymeric partner. This geometrical feature contributes to increased holding forces by mechanical interlocking in the direction of shear. In the case of PPS-CF composite, the formation of the nub is not accentuated because of the high stiffness of the carbon-fiber weave (Fig. 6D).

The microhardness field map of a sound FSpJ joint is shown in Fig. 7A, and the main microstructural characteristics to 7 K are shown in Fig. 7B. The microhardness of the metal is given in Vickers units and that of the polymer is given in MPa, which is a common unit for reporting polymer microhardness. For simplicity, only one half of each of the hardness maps is displayed, because the round spot is symmetrical.

Fig. 7B presents the AZ31 base material. Equiaxed grains resulting from the hot rolling fabrication are present along with second-phase particles (indicated by black arrows), which are at the grain boundaries and not homogeneously distributed within the grains. These Mg–Al intermetallic particles (see Section 3.1.1) are very brittle [25,37] and can act as crack nucleation sites. Furthermore, these particles can influence the dynamic recrystallization (DRX) mechanisms, retarding DRX grain growth by pinning and resulting in grain refinement [38]. No twins were observed in the as-received samples.

A region of the sample with a surface slightly deformed by the clamping ring is shown in Fig. 7C. Although its microstructure remains visually unchanged, the imposed deformation has increased the hardness to some extent, most likely by work hardening (Fig. 7A).

At the spot center (Fig. 7D–F), the microstructural zones generally found in friction spot metal welds [39] are seen. The stir zone (SZ) is characterized by very fine dynamic recrystallized grains.

The types of DRX processes in hexagonal close-packed Mg alloys are continuous (CDRX) (including twinning DRX [40,41]) at moderate temperatures (250–400 °C [42]) and discontinuous (DDRX) at temperatures above 400 °C [42].

Considering that the measured temperature in the tool (Fig. 5) varied between 400 °C and 440 °C, the very fine grains were most likely formed by DDRX. Additional investigations are being undertaken to better understand this phenomenon. When carefully examining the microstructure of the SZ (Fig. 7E and F), finer $Mg_{17}Al_{12}$ dispersed particles (black dots) can be observed. This is in agreement with the observation of Xunhong and Kuaishe [37], who addressed the refinement of these brittle secondary particles to particle breaking associated with the high shear rates in the SZ of friction stir-welded AZ31. The Hall–Petch effect related to grain size reduction increases the microhardness in the SZ. This can be observed in Fig. 7A in the regions within the SZ area, where the hardness is higher than that of the base material (85–90 HV in the SZ versus 58–60 HV in the base material).

The thermo-mechanically affected zone (TMAZ) is a thin transition zone between the SZ and the heat affected zone (HAZ). In this zone, grains start to plastically deform and DRX initiates, although to a lesser extent than in the SZ. A microstructure with partially refined grains is normally present (Fig. 7D and F). Finally, one can observe the presence of twins in the lower region of the metallic nub (Fig. 7H). The rate of dislocation generation in this region will overcome the annihilation rate, resulting in strain hardening. This effect is mainly due to the local process temperatures (200–225 °C, Fig. 5) associated with high levels of deformation induced by the vertical tool movement. This trend in local hardening is also found in friction stir welded AZ31 Mg alloy [37,44].

The details of the polymer–metal interface are shown in Fig. 7I and J. From these micrographs, two main geometrical patterns are observed: fiber and filler particle re-orientation, and porosity. As mentioned above, the PPS matrix closer to the polymer–metal interface will melt via conduction. Temperature measurements obtained in volumes close to the plasticized magnesium material (see thermocouples T1 and T4, Figs. 3 and 5) indicate that the temperature in the polymer–metal interface will easily exceed the

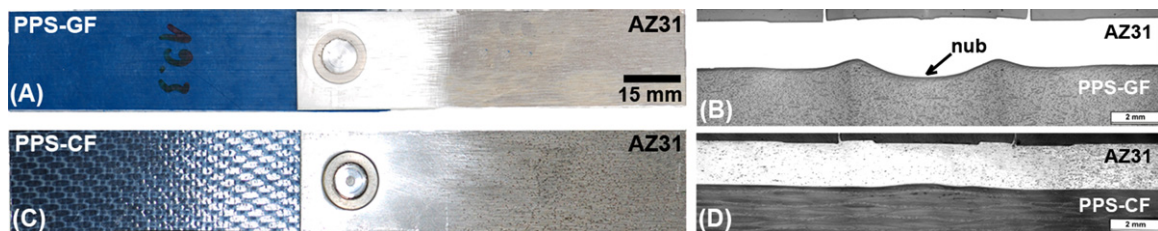


Fig. 6. (A) Surface appearance of a PPS-GF/Mg AZ31 single lap joint (3000 rpm, 0.25 mm, 8 s, 2 bar); (B) cross-sectional light optical macrograph of specimen in A; (C) surface appearance of a PPS-CF/Mg AZ31 single lap joint (specimen from Fig. 5) and (D) cross-section OM macrograph of specimen in C.

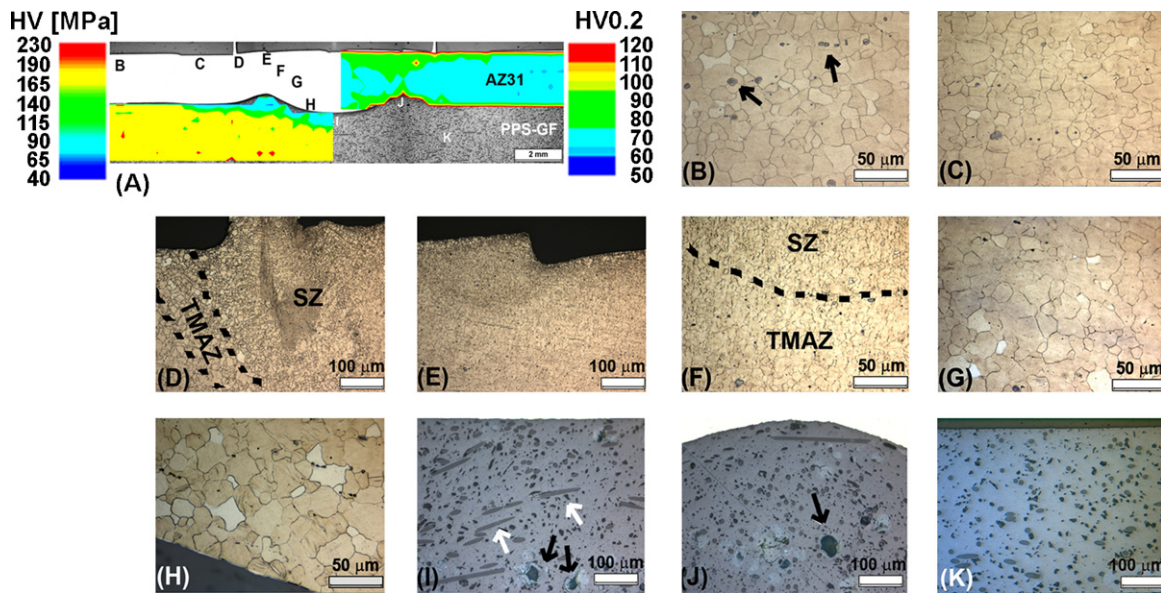


Fig. 7. Microstructure and hardness distribution of the spot joint in Fig. 6A and B: (A) diagram overlay of the non-etched cross section macrograph and microhardness maps; (B) the upper region of the AZ31 base material; (C) AZ31 volume below the clamping ring; (D) detail of the transition between TMAZ and stir zone; (E) center of the stir zone; (F) region showing the transition of the stir zone and TMAZ; (G) the central region of the HAZ; (H) interface between metal and polymer within the metallic nub; (I) consolidated polymer layer underneath the metallic nub; (J) consolidated polymer layer close to the metal polymer interface and (K) the upper portion of the base material polymeric plate.

melting point of the PPS matrix. As a result, re-orientation of the glass fibers (white arrows in Fig. 7I) in the direction of the polymeric material flow will be induced by the plunging of the metallic nub into the viscous polymer.

Few voids (see black arrows in Fig. 7F and I) are observed in the consolidated PPS layer close to the non-molten polymeric volume. Ma et al. [45] found that the thermal degradation in air of PPS starts at about 500 °C and is completed at 670 °C. Considering that the maximal process temperatures achieved are likely below 450 °C, the expected level of thermally degraded PPS is assumed to be very low, and thus, voids are unrelated to thermal degradation. The voids are likely to be the result of air trapped in the highly viscous molten polymer.

Nishihata et al. [46] studied the influence of annealing on the PPS crystallinity and tensile strength in air at 250 °C and 1 h. They observed that some annealed PPS grades experienced a reduction in strength. This behavior can be explained by a decrease in the degree of crystallinity related to chain cross-linking during annealing. PPS is slightly cross-linkable above its melting temperature in

the presence of air [45]. Cross-linking will lower the rate of nucleation and growth of crystallites, thereby reducing the strength and microhardness. The distribution of Vickers microhardness in the PPS-GF partner is shown in Fig. 7A. There is clearly a decrease in hardness in the consolidated layer and the adjacent heat-treated volume in comparison to the untreated polymer (100–140 MPa in the consolidated layer versus 170 MPa in the base polymer). This behavior might result from a decrease in the degree of crystallinity because of cross-linking induced by thermal effects during joint consolidation. Additional investigations are underway that aim to better explain this occurrence.

4.3. Global joint strength

Lap shear testing (Section 3.2.2) was performed to investigate static mechanical performance of the FSpJ joint. Examples of selected shear force–displacement curves are shown in Fig. 8A. To our knowledge, there are no available data in the literature addressing mechanical properties of overlap joints in PPS and AZ31.

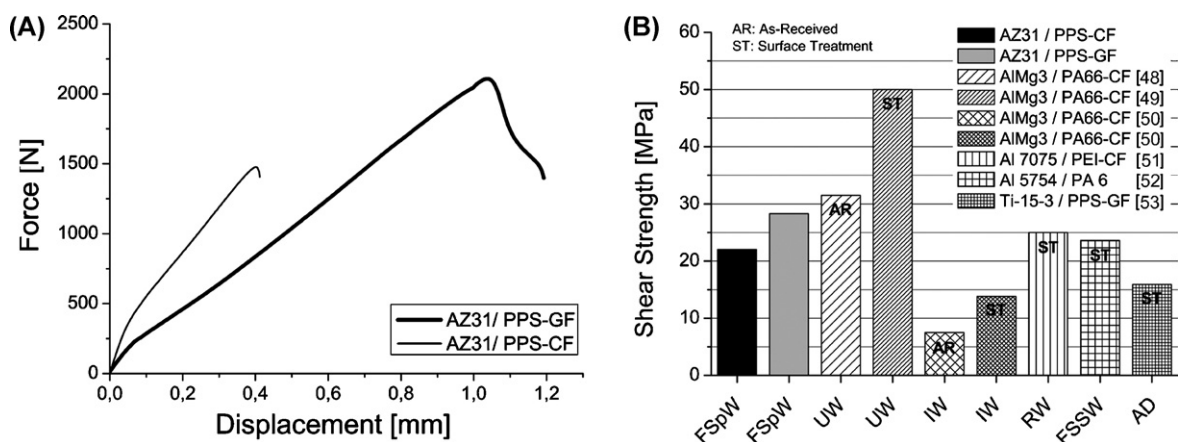


Fig. 8. (A) Example of force versus displacement curves for FSpW Mg AZ31/PPS-GF, PPS-CF joints (PPS-CF/AZ31: 1950 rpm, 0.25 mm plunge depth, 8 s, 2.5 bar; PPS-GF/AZ31: 3000 rpm, 0.25 mm plunge depth, 8 s, 2 bar); (B) histogram showing average ultimate shear strength of selected FSpJ joints and available techniques (UW: ultrasonic welding, IW: induction welding, RW: resistance welding, FSSW: friction stir spot welding, AD: direct adhesive bonding).

Table 6
State of the art in polymer–metal lap joints.

Joining process	Materials	Surface treatment	Process conditions	Testing method	Fracture type	Reference
FSpW	Mg AZ31/PPS-CF	Grinding SiC grid paper P1200 + acetone rinsing	1950 rpm, 0.25 mm plunge depth, 8 s, 2.5 bar	DIN EN 10002	Mixed cohesive/adhesive regime (composite)	–
FSpW	Mg AZ31/PPS-CF	Grinding SiC grid paper P1200 + acetone rinsing	3000 rpm, 0.25 mm plunge depth, 8 s, 2 bar	DIN EN 10002	Mixed cohesive/adhesive regime (polymer)	–
Ultrasonic welding	AlMg ₂ (1 mm)/PA 66-CF (2 mm)	As-received	Vibration amplitude: 40 μ m; axial force: 1.40 MPa; energy: 2160 J	Single lap joints (single specimens of 25 mm \times 70 mm)	Cohesive (composite)	[48]
Ultrasonic welding	AlMg ₂ (1 mm)/PA 66-CF (2 mm)	Corundum blasting + HNO ₃ pickling	Vibration amplitude: 37–43 μ m; axial force: 100–200 MPa; energy: 1700–2500 Ws	Single lap joints (single specimens of 25 mm \times 70 mm. Overlap: 25 mm \times 25 mm)	Cohesive (composite)	[49]
Induction welding	AlMg ₂ (1 mm)/PA 66-CF (2 mm)	Acetone wiping and corundum blasting + additional 100 μ m PA 66 film	Welding force: 0.5 MPa and 800 Hz	DIN EN 1465	Mixed cohesive/adhesive regime (composite)	[50]
Resistance welding	Al 7075-T6 (3 mm)/PEI-CF (3.14 mm)	Abrasion + degreasing + alkaline cleaning + phosphoric acid anodization (PAA)	Power: 90 kW/m ² ; welding time: 10 min	ASTM D-1002	Cohesive (composite)	[51]
Friction stir spot welding	Al 5754 (2 mm)/PA 66 (1.6 mm)	Aluminum: as-received/nylon heat treated in air at 125 °C/24 h.	Tool: steel, shoulder Φ 10 mm/pin Φ 2.5 mm	Single lap joints (specimens: 25.4 mm \times 100 mm. Overlap: 25.4 mm \times 25.4 mm)	Cohesive (polymer)	[52]
Adhesive bonding	Ti 15–3 (1.6 mm)/PPS-GF (2.5 mm). Adhesive: AF-3109-2K	Ti: sodium hydroxide anodization (SHA). Composite: corundum blasting	Curing: 150 °C/60 min/350 KPa	ASTM D-5868-95	Cohesive (composite)	[53]

As a result, an attempt was performed to compare FSpJ with the best shear strength results available in the literature on polymer composite/metal hybrid joints produced with different joining technologies and surface pre-treatments. For comparison purposes, FSpJ joint ultimate forces were converted to ultimate shear stress through the adoption of a nominal welding area corresponding to the outer sleeve diameter of the FSpJ tool (Φ 9 mm). This is a common procedure adopted in cases where the real joined area is not measurable. Fig. 8B summarizes the current performance of FSpJ in comparison with available techniques. Table 6 sums up the main characteristics of the joints presented in Fig. 8B.

Although a direct comparison of FSpW with data from the available literature was not possible, important conclusions can be drawn considering the observed similarities in joint geometry, testing procedures, and fracture mechanisms in the existing joining techniques. First, FSpJ joints without surface pre-treatment displayed comparable or better ultimate tensile strengths than those reported in the literature (see as-received ultrasonic and induction welded specimens, Fig. 8B). Secondly, FSpJ joints are even stronger than some joints produced with surface pre-treatment (compare as-received and surface-treated induction, resistance, friction stir spot welding and adhesive bonded joints). Thus, an additional increase in the strength of FSpJ joints is expected when applying surface pre-treatments. Balle et al. [49] and Velthuis et al. [50] have shown that simple mechanical surface pre-treatment on the metal component can improve the mechanical performance of polymer–metal overlap joints due to the creation of sufficient surface roughness, thereby increasing micro-mechanical interlocking. Current investigations of the influence of surface treatments for the magnesium/PPS-composite FSp joints, to be published separately, have indicated an average increase of about 50% in the joint lap shear strength when increasing the roughness of the magnesium partner from 0.75 μ m to 3.45 μ m by mechanical grinding.

The fracture surface analysis of the PPS-CF/AZ31 joint from Fig. 8A is presented in Fig. 9. A mixed cohesive–adhesive fracture

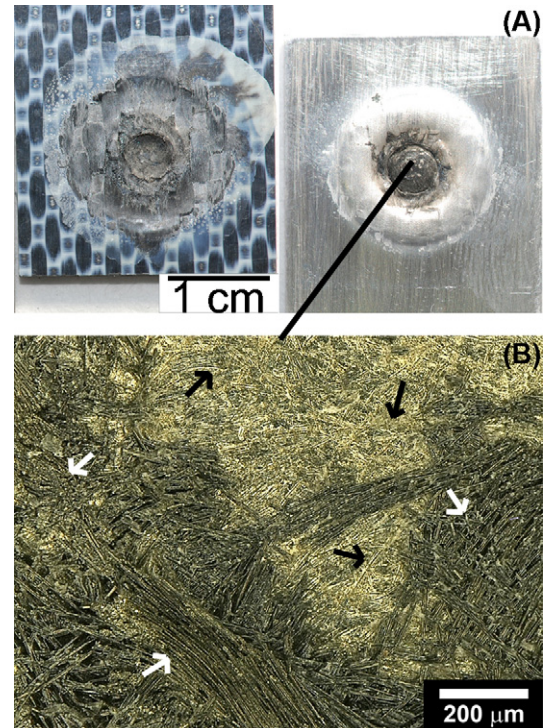


Fig. 9. (A) Overview of the fractured PPS-CF/AZ31 FSp lap joint in Fig. 8. (B) Infrared micrograph of the central region in the spot area of the magnesium plate.

regime is present. Cohesive fracture took place in the composite piece, which is identified by a partial polymer matrix and fiber attachment on the magnesium plate after testing (Fig. 9B, white arrows). Adhesive fracture took place in the polymer–metal interface, which is evident in the blank regions on the magnesium plate (Fig. 9B, black arrows). The partial presence of adhesive failure is an indication of the central role that adhesion forces play in joint formation.

5. Conclusions and final remarks

The current study has demonstrated that friction spot joining can be successfully used to join magnesium to thermoplastic composites. The peak temperatures were within 0.5–0.80T_m of the AZ31B, and within such a range, the PPS structure is changed by annealing. In this way, metallurgical and polymer physical–chemical transformations take place during joining. Dynamic recrystallization (grain refinement) in the stir zone and thermal changes in the PPS structure in the consolidated zone directly influence the microhardness distribution (local strength) of FSpj joints. These phenomena are still under investigation, and additional work will help to clarify the process/structure/properties relationships in FSpj of polymer–metal hybrid structures. Although the bonding mechanisms of FSpj are not yet well understood, there are strong indications that joining is accomplished by a mixed regime of surface mechanical interlocking (through micro and macro constraints related to the metallic nub) and adhesion between the metallic and consolidated polymeric layers, as well as direct partial fiber attachment on the metallic plate. The main advantages are as follows: short joining cycles, absence of emissions, operation simplicity, availability of commercial equipment, and good mechanical performance. The limitations include the following: only overlap configurations and spot geometries can be produced; the technique is not directly applicable to thermoset matrix composites (the use of an adhesive layer is required); and it is not adequate for very thick metallic partners (currently tested thicknesses are within 1–2 mm). The positive preliminary results of this work make FSpj an alternative joining technology for polymer–metals hybrid structures.

Acknowledgements

The authors would like to thank A. Hoppe for the preparation of metallographic specimens. The authors would like to acknowledge the financial support of the Helmholtz Association of Germany (Grant: Young Investigator Group “Advanced Polymer–Metal Hybrid Structures”).

References

- [1] B. Reinhold, K. Angermann, in: W. Krenkel (Ed.), *Verbundwerkstoffe (Composites)*, Wiley-VCH GmbH & Co. KGaA, Weinheim, 2009, pp. 27–38.
- [2] P. Juchmann, S. Wollf, in: K.U. Kainer (Ed.), *Magnesium*, Wiley-VCH GmbH & Co. KGaA, Weinheim, 2004, pp. 1006–1012.
- [3] A. Gavine, *Dream Team: An Efficient Test Program is Underway to Create an Efficient Aircraft*, Aerospace Testing International, 2005, pp. 39–43.
- [4] S.T. Peters, *Handbook of Composites*, second ed., Chapman & Hall, London, 1998, pp. 115–128.
- [5] R.G.S. Barsoum, *AMPTIAC – Quarterly* 7 (3) (2003) 55–61.
- [6] R. Stauber, in: W. Krenkel (Ed.), *Verbundwerkstoffe (Composites)*, Wiley-VCH GmbH & Co. KGaA, Weinheim, 2009, pp. 12–26.
- [7] F. Faupel, R. Willecke, A. Thran, *Mater. Sci. Eng. R* 22 (1998) 1–55.
- [8] R.W. Messler Jr., *Assembly Autom.* 20 (2) (2000) 118–128.
- [9] R.W. Messler Jr., *J. Thermoplast. Compos. Mater.* 17 (51) (2004) 51–75.
- [10] S.T. Amancio-Filho, J.F. dos Santos, *Polym. Eng. Sci.* 49 (8) (2009) 1461–1476.
- [11] C. Schilling, J.F. dos Santos, US Patent No. 6722556B2 (2004).
- [12] P.H.F. Oliveira, S.T. Amancio-Filho, J.F. dos Santos, E. Hage Jr., *Mater. Lett.* 64 (2010) 2098–2101.
- [13] S.T. Amancio-Filho, P.H.F. de Oliveira, C. Bueno, A. Hoppe, J.F. dos Santos, E. Hage Jr., *Proceedings for ANTEC 2010, Orlando World Center Marriott Resort & Convention Center, Orlando, FL, USA, May, 2010*.
- [14] S.T. Amancio-Filho, J.F. dos Santos, European Patent Application No. EP 09015014 (2009).
- [15] V. Kaese, L. Greve, S. Jüttner, M. Goede, S. Schumann, H. Friedrich, W. Holl, W. Ritter, in: K.U. Kainer (Ed.), *Magnesium*, Wiley-VCH GmbH & Co. KGaA, Weinheim, 2004, pp. 949–954.
- [16] B.L. Mordike, T. Ebert, *Mater. Sci. Eng. A* 302 (2001) 37–45.
- [17] J.A. Esparza, W.C. Davis, E.A. Trillo, L.E. Murr, *J. Mater. Sci. Lett.* 21 (2002) 917–920.
- [18] L. Commin, M. Dumont, J.-E. Masse, L. Barrallier, *Acta Mater.* 57 (2) (2009) 326–334.
- [19] Q. Yang, S. Mironov, Y.S. Sato, K. Okamoto, 7th International Friction Stir Welding Symposium, Awaji Yumebutai Conference Centre, Awaji Island, Japan, May, 2008.
- [20] H. Domininghaus, *Die Kunststoffe und ihre Eigenschaften*, fifth ed., Springer-Verlag, Berlin, 1998, pp. 887–906.
- [21] L.A. Berglund, in: S.T. Peters (Ed.), *Handbook of Composites*, second ed., Chapman & Hall, London, 1998, pp. 115–130.
- [22] J.A. Brydson, *Plastics Materials*, seventh ed., Butterworth-Heinemann, Oxford, 1999, pp. 593–596.
- [23] P. Mitschang, M. Blinzler, A. Wöginger, *Compos. Sci. Technol.* 63 (2003) 2099–2110.
- [24] M.M. Avedesian, H. Baker, *ASM Specialty Handbook, ASM International, Materials Park*, 1999, pp. 78–79.
- [25] J. Yan, Z. Xu, Z. Li, L. Li, S. Yang, *Scripta Mater.* 53 (2005) 585–589.
- [26] S.W. Xu, N. Matsumoto, S. Kamado, T. Honma, N. Saito, *Mater. Sci. Eng. A* 517 (2009) 354–360.
- [27] Techtron HPV PPS, Technical and data sheets, Quadrant Engineering Plastics Products, Germany, 2007.
- [28] Cetex PPS, Technical Data sheets, Tencate Advanced Composites, Netherlands, 2009.
- [29] ASTM E384–992e1, Standard Testing Method for Microindentation Hardness of Materials, ASTM International, USA, 2005.
- [30] F.J.B. Calleja, S. Fakirov, *Microhardness of Polymers*, Cambridge University Press, Cambridge, 2000, p. 238.
- [31] DIN EN 10002 Part 1, Tensile Testing of Metallic Materials – Method of Test at Ambient Temperature, DIN-Institut für Normung e.V., Berlin, Germany, 1991, p. 19.
- [32] DIN 53455, Prüfung von Kunststoffen, Zugversuch, DIN-Institut für Normung e.V., Berlin, Germany, 1981, pp. 241–248.
- [33] ASTM D 1002–05, Standard Test Method for Apparent Shear Strength of Single-Lap-Joint Adhesively Bonded Metal Specimens by Tension Loading (Metal-to-Metal), ASTM International (Beuth Verlag GmbH), Berlin, Germany, 2005, p. 5.
- [34] T. Nagasawa, M. Otsuka, T. Yokota, T. Ueki, in: H.I. Kaplan, J. Hryn, B. Clow (Eds.), *Magnesium Technology 2000, The Minerals, Metals & Materials Society*, Nashville, TN, 2000, pp. 383–387.
- [35] Y.V.R.K. Prasad, K.P. Rao, *Adv. Eng. Mater.* 9 (7) (2007) 558–565.
- [36] W. Xunhong, W. Kuaishe, *Mater. Sci. Eng. A* 431 (2006) 114–117.
- [37] S.W. Xu, N. Matsumoto, S. Kamado, T. Honma, Y. Kojima, *Scripta Mater.* 61 (2009) 249–252.
- [38] A.A.M. da Silva, J.F. dos Santos, T.R. Rosendo, F.D. Ramos, C.C.P. Mazzaferro, M.A.D. Tier, L. Bergmann, J.A.E. Mazzaferro, T.R. Strohaecker, Performance evaluation of 2-mm thick alclad AA2024 T3 aluminium alloy friction spot welding, Society of Automotive Engineering – SAE, 2007, Paper No. 07ATC-103.
- [39] O. Sitdikov, R. Kaibyshev, T. Sakai, *Mater. Sci. Forum* 419–422 (2003) 521–526.
- [40] X. Yang, H. Miura, T. Sakai, *Mater. Sci. Forum* 419–422 (2003) 515–520.
- [41] S.M. Fatemi-Varzaneh, A. Zarei-Hanzaki, H. Beladi, *Mater. Sci. Eng. A* 456 (2007) 52–57.
- [42] C.I. Chang, X.H. Du, J.C. Huang, *Scripta Mater.* 57 (2007) 209–212.
- [43] C.-C.M. Ma, H.-C. Hsia, W.-L. Liu, J.-T. Hu, J. Thermoplast. Compos. Mater. 1 (1998) 39–49.
- [44] N. Nishihata, T. Koizumi, Y. Ichikawa, T. Katto, *Polym. Eng. Sci.* 38 (3) (1998) 403–408.
- [45] F. Balle, G. Wagner, D. Eifler, *Adv. Eng. Mater.* 11 (2009) 35–39.
- [46] F. Balle, G. Wagner, D. Eifler, in: M. Pohl (Ed.), *Werkstoffprüfung 2004, Werkstoff-Informationsgesellschaft GmbH, Frankfurt*, 2004, pp. 329–334.
- [47] R. Velthuis, P. Mitschang, S. Emrich, M. Kopnarski, *J. Thermoplast. Compos. Mater.* 22 (6) (2009) 767–801.
- [48] C. Ageorges, L. Ye, J. Thermoplast. Compos. Mater. 14 (2001) 449–475.
- [49] K.N. Balakrishnan, H.T. Kang, P.K. Mallick, SAE Technical Paper Series, SAE, 2007, Paper No. 2007-01-1701.
- [50] P. Molitor, T. Young, *Int. J. Adhes. Adhes.* 22 (2002) 101–107.